The Astrophysical Journal: submitted May 9, accepted July 11, 1997
Preprint typeset using LaTeX style emulateapj v. 04/03/99

AN X–RAY SIZE–TEMPERATURE RELATION FOR GALAXY CLUSTERS: OBSERVATION AND SIMULATION

Joseph J. Mohr[1,2] & August E. Evrard[1,3]
[1]Department of Physics & [2]Department of Astronomy, University of Michigan, Ann Arbor, MI 48109
[3]Institut d'Astrophysique, 98bis Blvd Arago, 75014 Paris, France
The Astrophysical Journal: submitted May 9, accepted July 11, 1997

ABSTRACT

We show that galaxy clusters conform to a tight relation between X–ray isophotal size R_I and emission weighted intracluster medium (ICM) temperature $\langle T_X \rangle$. The best fit relation for 41 members of an X–ray flux limited cluster sample is: $\log R_I = (0.93 \pm 0.11) \log(\langle T_X \rangle / 6\,\mathrm{keV}) - (0.08 \pm 0.01)$; intrinsic scatter in size about the relation is 15%, and for 30 clusters with $\langle T_X \rangle > 4$ keV the scatter is reduced to 10%. The existence of the size–temperature (ST) relation indicates the ICM structure is a well behaved function of $\langle T_X \rangle$. We use an ensemble of gasdynamic simulations to demonstrate that a cluster population experiencing present epoch growth nonetheless conforms to an ST relation with scatter similar to that observed; the simulations also exhibit a tight relation between M_{vir} and $\langle T_X \rangle$, providing the suggestion that a similar relation holds for observed clusters. We use the scatter in R_I to estimate limits on the *rms* variation in ICM mass fraction δf_{ICM} at constant $\langle T_X \rangle$: $\delta f / f_{ICM} \leq 22\%$ ($\leq 14\%$ for clusters with $\langle T_X \rangle > 4$ keV). It appears that a mechanism like feedback from galaxy winds, which introduces systematic structural changes in the ICM, is required to reproduce the observed slope of the ST relation.

Subject headings: galaxies: clusters: general — intergalactic medium — X–rays: galaxies

1. INTRODUCTION

Ongoing cluster growth at the present epoch is an observational fact (e.g. Fabricant et al. 1986, 1989, Zabludoff & Zaritsky 1995, Henry & Briel 1995, Mohr, Geller & Wegner 1996); large studies employing varied techniques indicate that 30–70% of clusters exhibit evidence for recent mergers (Geller & Beers 1982, Dressler & Shectman 1988, Jones & Forman 1992, Mohr et al. 1995). A theoretical framework for understanding this growth has emerged, and structure formation simulations within a range of favored cosmological models produce clusters which exhibit merger signatures similar in detail and frequency to those observed (Mohr et al. 1995, Buote & Xu 1997).

Yet, recent numerical work indicates that even though clusters are growing at the present epoch, they are, on average, regular objects with temperatures and masses tightly correlated through the virial theorem (Evrard, Metzler & Navarro 1996, Schindler 1996, Roettiger, Burns & Loken 1996). Direct observational tests of these results are difficult, but analyzing relations between ICM structural parameters and temperature provides an alternative means of testing cluster regularity. The well known X–ray luminosity–temperature ($L_X - \langle T_X \rangle$) relation (e.g. Smith, Mushotzky & Serlemitsos 1979, Mitchell et al. 1979, David et al. 1993, Mushotzky & Scharf 1997) is one observational indicator of cluster regularity, but the scatter around the relation is quite large. The scatter is largely due to varying degrees of excess core emission associated with cooling flows (Fabian *et al.* 1994).

Here we report a tight relation between cluster isophotal size R_I and mean, emission weighted temperature $\langle T_X \rangle$ that we uncovered in an ongoing morphological analysis of a large, X–ray flux limited cluster sample. This ST relation for observed clusters indicates a high degree of regularity, suggests the existence of a mass–temperature correlation, and provides new constraints on theories of the interactions between galaxies and the ICM. This newly discovered ST relation may ultimately lead to more accurate estimates of cluster baryon fractions and tighter constraints on the cosmic density parameter Ω_0 (e.g. White et al. 1993, Evrard 1997).

Section 2 contains a description of the data reduction, analysis and the observed ST relation. We then use an ensemble of numerical simulations to examine the ST relation in a cluster population experiencing present epoch growth (§3). In Section 4, we discuss sources of scatter about the relation, estimate upper limits on the variation in ICM mass fraction f_{ICM} , and discuss the slope of the ST relation. Section 5 contains a discussion of our conclusions.

2. OBSERVATIONS

The cluster sample contains members of the X–ray flux limited group of 55 clusters defined by Edge *et al.* (1990). Archival ROSAT Position Sensitive Proportional Counter (PSPC) images of 47 of these clusters are available online through the High Energy Astrophysics Science Archive Research Center (HEASARC). We reduce these images using PROS and Snowden analysis software (Snowden et al. 1994). The final image for each observation is the sum of individually flatfielded subimages from the Snowden bands R4 through R7, corresponding to photon energies 0.44–2.04 keV. We exclude time intervals with master veto rates higher than 220 cts/s, and exclude other high background time intervals (typically $\leq$5 min excluded) whose inclusion would degrade the detection significance of a source 10% as bright as the background (Pildis, Bregman & Evrard 1995). We combine multiple images of a cluster using the positions of bright X–ray point sources where possible, or alternatively, the image header pointing positions. Finally, we remove obvious point sources from the unsmoothed images (we do not remove possi-

ble point source components coincident with the extended emission typical of cluster cooling flows, as in NGC 1275, for example) and then Gaussian smooth ($\sigma = 2$ pixels). The pixel scale is $14''.947$, and the effective angular resolution is $FWHM \sim 1.5'$. We correct the cluster images for $(1+z)^4$ cosmological dimming, but do not make galactic absorption or K corrections (discussed in more detail below).

We define the cluster size R_I using the area A_I of the largest region enclosed by the isophote I.

$$R_I = \sqrt{A_I/\pi} \tag{2-1}$$

This approach deals consistently with clusters that are not azimuthally symmetric because of recent mergers, and produces a tighter relation than would azimuthal averaging; in addition, I can be chosen so that R_I is unaffected by the central surface brightness excesses typical of cooling flows. The isophote I is the cluster surface brightness, and we determine the X–ray background I_B using annuli well outside the X–ray bright cluster region (typically $38'$ from the cluster center with $\sim 8'$ extent). We estimate I_B as the (sigma clipped) mean value of the pixels within the annulus, and we use the width of the distribution around I_B to estimate the uncertainty. For the isophotes I we use, the uncertainty in R_I is primarily due to the background uncertainty. We conservatively estimate the uncertainties in R_I to be $\sigma_R = (R_{I_-} - R_{I_+})/2$ where $I_{+/-} = I \pm I_B/10$. The internal estimate of the uncertainty in I_B is significantly smaller than 10% in all cases.

We use published, emission weighted, mean temperatures $\langle T_X \rangle$ for each cluster. There are 42 clusters in the Edge sample with PSPC images and published $\langle T_X \rangle$ with uncertainties. Roughly half of these temperatures are from *Einstein* MPC observations (David et al. 1993), but where possible we substitute more accurate *Ginga*, *ASCA*, or ROSAT PSPC temperatures (*Ginga*— Day et al. 1991, Allen et al. 1992, Johnstone et al. 1992, David et al. 1993, Hughes et al. 1993, Arnaud & Evrard 1997; *ASCA*— Henriksen & Markevitch 1996, Markevitch 1996, Matsuzawa et al. 1996, Tamura et al. 1996, Markevitch & Vikhlinin 1997; PSPC— David, Jones & Forman 1996). We exclude the Virgo cluster from our analysis because bright, cluster emission extends beyond the 2° PSPC field of view. Thus, our final sample contains 41 clusters.

The observational data for this sample are displayed in Table 1; the cluster name, effective PSPC exposure time t_{exp}, background brightness I_B, emission weighted mean temperature $\langle T_X \rangle$, and designation as cooling flow cluster are listed. We designate those clusters with central cooling times significantly below 10 Gyr (Edge, Stewart & Fabian 1992) as cooling flow clusters.

Figure 1 contains a plot of the 41 clusters in $\log R_I$ and $\log \langle T_X \rangle$ for $I = 1.93 \times 10^{-3}$ cts/s/arcmin^2. A linear fit to the sample (minimizing the sum of the orthogonal residuals from the relation) yields

$$\log R_I = \ (0.93 \pm 0.11)\ \log \frac{\langle T_X \rangle}{6\,\mathrm{keV}} - \ (0.08 \pm 0.01). \tag{2-2}$$

The *rms* scatter in $\log R_I$ about this relation is $\delta \log R_{raw} = 0.084$. The coefficient uncertainties reflect the half width of the 68% confidence region determined by bootstrap resampling.

We analyze the ST relation in the PSPC sample over a factor of 8 in surface brightness (see Table 2 and §3.2); varying I primarily changes the zeropoint b of the ST relation. The integrity of the relation is preserved until I reaches values comparable to the peak surface brightnesses of some clusters.

The uncertainties in $\langle T_X \rangle$ are large enough to contribute to the observed scatter. We estimate the intrinsic scatter in $\delta \log R_I$ by subtracting the temperature contribution in quadrature. We find $\Delta(\delta \log R_I) = 0.93 * RMS(\sigma_T/T_X/\ln 10) = 0.054$. Thus, the intrinsic scatter is approximately $\delta \log R_{int} = 0.064$. Fig. 1 gives the impression that the scatter increases at lower temperature; fitting only those 30 clusters with $\langle T_X \rangle > 4$ keV leads to an ST relation $\log R_I = (0.82 \pm 0.14) \log(\langle T_X \rangle / 6\,\mathrm{keV}) - (0.07 \pm 0.02)$, with raw/intrinsic scatter of 0.067/0.041. Thus, the slope of the ST relation for hot clusters is slightly shallower than that for the whole population, and the scatter is smaller by 50%.

3. SIMULATIONS

We further examine the ST relation using a set of 48 high resolution N–body plus gas dynamics simulations, to be described in detail elsewhere (Mohr & Evrard 1997). In summary, the cluster simulations are carried out within four different cold dark matter (CDM) dominated cosmologies (1) SCDM ($\Omega = 1$, $\sigma_8 = 0.6$, $h = 0.5$), (2) OCDM ($\Omega_0 = 0.3$, $\sigma_8 = 1.0$, $h = 0.8$), (3) LCDM ($\Omega_0 = 0.3$, $\lambda_0 = 0.7$, $\sigma_8 = 1.0$, $h = 0.8$), and (4) ZCDM ($\Omega = 1$, $\sigma_8 = 1.0$, $h = 0.5$) with power spectrum consistent with a CDM $\Gamma = 0.24$ transfer function (Davis et al. 1985). Here $H_0 = 100h$ km/s/Mpc and σ_8 is the power spectrum normalization in $8h^{-1}$ Mpc spheres. The baryon density is a fixed fraction of the total $\Omega_b = 0.2\Omega_0$. Within each of these models, we use two 128^3 N–body only simulations of cubic regions with scale ~ 400 Mpc to determine sites of cluster formation. Within these initial runs the virial regions of clusters with Coma–like masses of 10^{15} $M_\odot$ contain $\sim 10^3$ particles.

Using the N–body results for each cosmological model, we choose clusters for additional study. We zoom in on these clusters, resimulating them at higher resolution with gas dynamics and gravity on a 64^3 N–body grid. The simulation scheme is P3MSPH (Evrard 1988), and radiative cooling is ignored. These clusters have masses which varying by an order of magnitude. The scale of the simulated region surrounding each cluster are in the range 50–100 Mpc, and vary as $M_{halo}^{1/3}$, where M_{halo} is approximately the mass enclosed within the present epoch turn around radius. Thus, the 48 simulated clusters in our final sample have similar fractional mass resolution; the spatial resolution varies from 125–250 kpc. We create X–ray images and temperature maps for further analysis following procedures described in Evrard (1990).

Fig. 2A is a plot of the ST relation for the simulated clusters (with $I = 1.62 \times 10^{-3} h_{50}^3$ cts/s/arcmin^2). Clusters from the four cosmological models are plotted with different point styles, each appears three times from orthogonal projections. The best fit relation for the SCDM model is $\log R_I = 0.70 \log(\langle T_X \rangle / 6\,\mathrm{keV}) + 0.119$ and the scatter around this fit is $\delta \log R = 0.042$; Table 2 contains the relations and scatter for all models; the level of scat-

ter is typically somewhat smaller than the observed value. Only ZCDM clusters have a higher scatter than our estimate of the intrinsic scatter in the observed sample; the higher scatter is caused by a few ongoing major mergers at high $\langle T_X \rangle$.

The scatter around the ST relation in the simulated populations is due to projections of clusters along the line of sight, small equilibrium departures, and small ($\sim 5\%$) intrinsic fractional f_{ICM} variations which exist because of different formation histories. On average, these clusters reached half of their present epoch mass at look–back epochs $0.33t_0$: $0.35t_0$: $0.42t_0$: $0.44t_0$: for Z:S:O:LCMD, where t_0 is the age of the universe in each model. The S, O and LCDM clusters are morphologically similar to observed clusters, and the ZCDM clusters exhibit somewhat more evidence for recent mergers than the other three models and the observed clusters (Mohr & Evrard 1997).

4. ANALYSIS

The existence of the ST relation in this large, approximately flux limited cluster sample demonstrates that the ICM structure is a well behaved function of $\langle T_X \rangle$. After correcting for measurement uncertainties, the scatter of the clusters about the ST relation is similar to the scatter of bright ellipticals around the fundamental plane (e.g., Jørgensen, Franx & Kjærgaard 1996, Mohr & Wegner 1997). To further understand this relation, we examine sources of scatter about it, and then we use the scatter to place upper limits on variations in the ICM mass fraction f_{ICM} . We also examine the ST relation slope, which provides information about the physical processes affecting the ICM structure.

4.1. *Scatter About the ST Relation*

There are several sources of scatter in the ST relation besides the measurement uncertainties discussed in §2. These include: (1) variations in galactic N_H absorption, (2) departures from equilibrium, (3) projections of physically unassociated clusters along the line of sight, and (4) dark matter and ICM structural variations at constant $\langle T_X \rangle$.

The contribution from variations in galactic N_H is insignificant. We use PROS tasks to calculate surface brightness correction factors for galactic absorption at 1 keV for our cluster sample. We find that these correction factors have a mean of 1.17 and an *rms* variation of 6.8% about this mean value for the 41 clusters. Typical surface brightness profiles are rather steep $I(R) \propto R^{-3}$ (e.g. Jones & Forman 1984, Mohr et al. 1995), so $\delta \log R = \frac{1}{3} \delta \log I$ and the variation in galactic absorption along the lines of sight to these clusters is expected to contribute scatter at the level of $\sim$2.3%. Galactic absorption is approximately 45% more effective at 0.5 keV, the low energy end of our bandwidth (and, of course, less effective at 2.0 keV), so the maximal contribution to the ST relation scatter from variations in galactic N_H is $\sim$3.3%.

Departures from equilibrium contribute significantly to the scatter. Two clusters of similar mass about to merge in the plane of the sky will be 40% too large in R_I for their $\langle T_X \rangle$. The scatter about the ST relations exhibited by the simulations described in §3 is an indicator of the expected contribution from equilibrium departures and projection effects in cluster populations still merging at the present epoch.

Equilibrium dark matter and ICM structural variations at a particular temperature will also contribute to the ST relation scatter. N–body simulations indicate that the dark matter structure of clusters is a regular function of mass, and that mild variations among clusters with similar mass are attributable to different formation times (Navarro, Frenk & White 1996). Again, major mergers present exceptions, but do not dominate the local population. The ICM distribution of clusters with similar masses has not been as extensively studied as the dark matter, but the experiments shown here and below suggest that the ICM structure is a well behaved function of cluster mass or temperature, even in the presence of galactic winds (Metzler & Evrard 1997). Other sources of variation in the ICM distribution or gas mass fraction are possible. One source is radiative cooling, which leads to strong emission excesses or cooling flows in cluster centers (Jones & Forman 1984, Fabian 1994).

We examine the effects of cooling flows by dividing our cluster sample into those with cooling times (t_{cool} significantly less than 10 Gyr) short enough that cooling flows should exist in the core, and those with longer cooling times (Edge, Stewart & Fabian 1992). We find that the best fit ST relation for the 18 cooling flow clusters (see Table 1) has a slope $m = 0.93 \pm 0.16$ and a zeropoint $b = -0.07 \pm 0.02$; the relation for the 23 non–cooling flow clusters has $m = 1.00 \pm 0.21$ and $b = -0.09 \pm 0.02$. The raw/intrinsic scatter about these two relationships is $\delta \log R_I = 0.086/0.071$ for the cooling flow clusters and $\delta \log R_I = 0.083/0.061$ for the non–cooling flow clusters. These two relations are indistinguishable and the scatter about each is comparable; thus, for the present sample of 41 clusters there is no indication that the ST relation is sensitive to the presence of cooling flows.

4.2. *Upper Limit on ICM Mass Fraction Variations*

By assuming the observed scatter in the ST relation is caused solely by varying ICM mass fraction f_{ICM} at constant $\langle T_X \rangle$, we estimate an upper limit on these variations. The surface brightness profiles of both real and simulated clusters are generally well fit with the standard, isothermal β–model

$$I(R) = A \Lambda \rho_0^2 R_c \left[1 + (R/R_c)^2\right]^{-3\beta+1/2} \qquad (4\text{-}1)$$

where ρ_0 is the central ICM density, Λ is the specific emissivity, R_c is a core radius, β is the variable slope, and A is a constant with some β dependence (Cavaliere & Fusco–Femiano 1978). We use this model as a guide to understanding the ST relation (but the relationship below can be derived independent of the β model). Within this framework, the ICM mass fraction is

$$f_{ICM} = \frac{4\pi \rho_0 R_c^3 \int_0^{R_{vir}/R_c} d\lambda \, \lambda^2 (1+\lambda^2)^{-3\beta/2}}{M_{vir}} \qquad (4\text{-}2)$$

where R_{vir} is the virial radius encompassing a fixed density contrast. Outside the core, the surface brightness scales as

$$I(R) \; = \; C \; f_{ICM}^2 \; R^{-6\beta+1} \qquad (4\text{-}3)$$

where the constant C incorporates the ICM structural information of equation (4-2). If clusters of a given tempera-

ture are structurally similar, then the scatter in the isophotal radii at constant $\langle T_X \rangle$ places an upper limit on variations in the gas fraction $\delta \log f_{ICM} \leq [(6\beta - 1)/2] \delta \log R_I$. This inequality can be broken if structural variations (variations in C) are anti–correlated with variations in f_{ICM}; we assume here that this is not the case. Qualitatively, such an anti–correlation would require gas–poor clusters to be more centrally concentrated (and vice–versa), a situation at odds with traditional expectations.

For the typical value $\beta = 2/3$ (Jones & Forman 1984, Mohr et al. 1995), $\delta \log f_{ICM} \leq 1.5 \delta \log R_I$, and the intrinsic scatter in $\log R_I$ limits fractional gas variations to $\delta f / f_{ICM} \leq 22\%$. The limit drops to $\delta f / f_{ICM} \leq 14\%$ for the 30 clusters hotter than 4 keV.

The scatter about the ST relation in the simulated clusters includes a contribution from variations in f_{ICM} within the virial radius. This contribution is rather small: $\delta f / f_{ICM} \simeq 4\%$ within r_{500}, the radius within which the mean cluster density is 500 times the critical density. Thus, other effects such as departures from equilibrium and projections dominate the scatter. Assuming these effects exist to a similar degree in the observations, then the similar scatter in the simulations and the observed clusters with $\langle T_X \rangle > 4$ keV indicates that gas fraction variations within hot clusters are very small, perhaps as small as 4%. This argument does not apply for cooler clusters, which exhibit larger scatter about the ST relation.

4.3. *Slope of the ST Relation*

The steeper observed slope $m = 0.93 \pm 0.11$, compared to $0.61 \leq m \leq 0.81$ in the simulations, suggests structural differences in real clusters compared to this set of models. Radiative cooling is not included in the simulations, but the similarity of the ST relation in clusters with and without cooling flows indicates this is not the cause of the slope differences. Possible explanations include systematic trends in the overall gas fraction f_{ICM} and/or systematic variations in the ICM distribution (as measured by β) with $\langle T_X \rangle$.

The observed cluster sample provides evidence that shallower surface brightness profiles lead to steeper ST relations. Table 2 lists the best fit slope m and zeropoint b for the observed clusters over a factor of 8 variation in I. Along with the expected zeropoint decrease with brightening I, there is a tendency for a steeper slope. This steepening is related to the shallower surface brightness profiles (smaller effective β) at brighter isophotes. Simulations from the four cosmological models provide additional evidence that shallower surface brightness profiles generally lead to steeper ST relation slopes; the mean β's of the Z:S:L:OCDM are are 0.67:0.73:0.77:0.81 and the m's are 0.81:0.70:0.72:0.61. Thus, the steeper observed ST relation may simply be an indication of a more extended ICM distribution in the observations than in the simulations.

Galactic winds are one physical process expected to introduce systematic ICM structural variations. In such a model, star formation within galaxies results in supernovae (SNe) driven winds which expell gas, and the expelled gas has the orbital kinetic energy of its parent galaxy plus the energy imparted by the SNe. This non–gravitational source of energy is expected to be more important in low $\langle T_X \rangle$ clusters where the orbital energies are smaller. We examine the effects of galactic winds on the ST relation using an ensemble of clusters from simulations which include galaxy feedback (Metzler & Evrard 1994; 1997). The simulated cluster ensemble contains two populations; one population of 18 clusters evolved consistent with an SCDM model and another population with the same initial conditions and cosmological parameters, but with galaxy feedback modeled by discrete gas ejection totalling half the initial galaxy mass between $z = 4.5$ and the present. This extreme ejection model is intended to estimate the maximal effect of galaxy feedback.

Fig. 2B is a plot of the effects of galaxy feedback on the ST relation. The slope of the best fit ST relation for the clusters with no feedback (dotted line) is $m = 0.69$, consistent with the SCDM slope in our simulations (see Table 2). The slope for clusters simulated with ejection (solid line) is $m = 0.99$, somewhat steeper than the slope of our PSPC sample. This demonstrates that galaxy feedback can cause the structural changes required to match the slope of the observed ST relation. Structural changes include shallower surface brightness profiles (smaller β) and lower overall gas fractions with decreasing $\langle T_X \rangle$, as discussed in Metzler & Evrard (1997). Fig. 2B makes clear that, as expected, ejection has the greatest effect on the lowest mass clusters.

The tendency for low $\langle T_X \rangle$ clusters to have shallower surface brightness profiles is well known (e.g., Mohr et al. 1995); our sample of 41 clusters exhibits this general trend. Fig. 3 contains a plot of the slope of the surface brightness profile β_{eff} measured over the region of the cluster used to calculate R_I . The Spearman rank correlation coefficient (Press et al. 1992) for $\langle T_X \rangle$ and β_{eff} is $r_s = 0.54$ with a correlation significance of 99.97%. β_{eff} is a two dimensional generalization of β, and like R_I , is measured without azimuthal averaging; moreover, β_{eff} reflects the local slope of the surface brightness profile and so is independent of the cluster core radius. Briefly, to calculate the values in Fig. 3 we determine the area A_l enclosed by the isophote $I_l = 1.29 \times 10^{-3}$ cts/s/arcmin^2 (chosen to be somewhat fainter than the I used to calculate R_I), and then calculate the isophote I_h which encloses the area A_h which is chosen to be $A_l/2$. This provides two isophotes and two areas, and so we then calculate the effective slope of the surface brightness profile between I_l and I_h

$$\beta_{eff} = \frac{1}{3} \left(\frac{\log (I_h / I_l)}{\log (A_l / A_h)} + \frac{1}{2} \right) \qquad (4\text{-}4)$$

This form follows directly from the expression $I(R) \propto R^{-6\beta_{eff}+1}$. The trend of falling β_{eff} with $\langle T_X \rangle$ is qualitatively consistent with the effects of galaxy feedback.

5. DISCUSSION

We use observations of the 41 members of an X–ray flux limited cluster sample with PSPC observations and published $\langle T_X \rangle$ (except Virgo) to demonstrate that nearby clusters conform to a tight relation between X–ray isophotal size and cluster temperature. The intrinsic scatter in size at fixed temperature is only 15% (10% for clusters with $\langle T_X \rangle > 4$ keV). The existence of the ST relation indicates that the ICM structure outside the core regions is a well behaved function of $\langle T_X \rangle$ and suggests a tight correlation between $\langle T_X \rangle$ and M_{vir} as seen in our simulations

and others (Evrard, Metzler & Navarro 1996, Schindler 1996, Roettiger, Burns & Loken 1996).

The ST relation is significantly tighter than the $L_X - \langle T_X \rangle$ relation for this cluster sample. The scatter (corrected for temperature uncertainties) in 2–10 keV X–ray luminosity (David et al. 1993) around the best fit relation for these 41 clusters is $\delta L_X / L_X = 52\%$. (We use the same set of temperature measurements in both cases.) The factor of 3.5 larger scatter in the $L_X - \langle T_X \rangle$ relation reflects the sensitivity of L_X to cluster core properties (Fabian et al. 1994). When restricted to weak cooling flow clusters — those with inferred cooling flow rates below 100 $M_\odot$ yr^{-1} — the $L_X - \langle T_X \rangle$ relation displays a much smaller dispersion, and inferred gas fraction variations from a sample of 24 clusters are consistent with the limits set by this analysis (Arnaud & Evrard 1997). The narrow scatter in the ST relation indicates that structural regularity exists outside the core at observationally viable surface brightness levels.

Our cluster sample provides no evidence that cooling flows significantly affect the ST relation. The 13 clusters with central cooling times significantly below 10 Gyr exhibit a best fit slope, zeropoint, and scatter which are statistically indistinguishable from those for the 18 other clusters. The zeropoint differences between these two ST relations indicate that $\langle T_X \rangle$ in cooling flow clusters is biased low by $\sim 5 \pm 7\%$, consistent with previous estimates of ∼10–20% (Fabian et al. 1994).

The scatter around the ST relation is comparable to that of the half light radius of elliptical galaxies around the fundamental plane (e.g. Jørgensen, Franx & Kjærgaard 1996, Mohr & Wegner 1997); an obvious use of the ST relation is as a distance indicator. Knowledge of $\langle T_X \rangle$ and an apparent isophotal size predicts the cluster distance with an uncertainty limited by the scatter in R_I ($\sim 10\%$ for hot clusters). We are currently evaluating the promise of this relation as a distance indicator at intermediate redshift.

The scatter about the best fit ST relation for observed clusters provides an upper limit on the *rms* variation in cluster ICM mass fraction at a common temperature $\langle T_X \rangle$. Ignoring possible correlations between cluster structural changes and f_{ICM} variations, we find upper limits $\delta f / f_{ICM} \leq 22\%$ ($\leq 14\%$ for $\langle T_X \rangle > 4$ keV).

We use 48 cluster simulations within 4 cosmological models to demonstrate that cluster populations experiencing growth at the present epoch exhibit ST relations with scatter similar to that observed above $\langle T_X \rangle > 4$ keV: $\delta R_I / R_I \simeq 10\%$. Only a small contribution to the scatter in the simulations is from f_{ICM} variations, suggesting that the ICM mass fraction in hot clusters may be limited to $\lesssim 5\%$ variation within their virial regions. Implications for hierarchical models of galaxy formation remain to be explored.

The slope of the ST relation for the PSPC clusters is steeper than the slope in our simulations. We use numerical simulations (Metzler & Evrard 1994, 1997) to show that galaxy feedback introduces the kinds of ICM structural changes required to steepen the ST relation. The changes include shallower surface brightness profiles and lower f_{ICM} with decreasing $\langle T_X \rangle$. A decrease in β with $\langle T_X \rangle$ (see Fig. 3) and a reduction of f_{ICM} in low $\langle T_X \rangle$ systems (David, Jones & Forman 1995, dell'Antonio, Geller & Fabricant 1995) have been observed. Galactic feedback is a promising mechanism for creating the observed, structural differences between low and high $\langle T_X \rangle$ clusters.

We are very grateful to C. Metzler for providing images of his simulations, M. Arnaud for providing $\langle T_X \rangle$ measurements prior to publication, M. Geller for comments on the paper, and D. Richstone for stimulating discussions. We thank the referee for helpful comments. This research has made use of the NASA/GSFC HEASARC Online Service, and has been supported by NASA through grants NAG5–3401 and NAGW–2367. AEE acknowledges support from the CIES and CNRS of France during a sabbatical stay at IAP.

REFERENCES

Allen, S. W., Fabian, A. C., Johnstone, R. M., Nulsen, P. E. J. & Edge, A. C. 1992, MNRAS, 254, 51
Arnaud, M. & Evrard, A. E. 1997, in preparation
Buote, D. A. & Xu, G. 1997, MNRAS, 284, 439
Cavaliere, A. & Fusco–Femiano, R. 1978, A&A, 70, 677
David, L. P., Slyz, S. C., Forman, W., Vrtilek, S. D. & Arnaud, K. A. 1993, ApJ, 412, 479
David, L. P., Jones, C. & Forman, W. 1995, ApJ, 445, 578
David, L. P., Jones, C. & Forman, W. 1996, ApJ, 473, 692
Davis, M., Efstathiou, G., Frenk, C. S. & White, S. D. M. 1985, ApJ, 292, 371
Day, C. S. R., Fabian, A. C., Edge, A. C., Raychaudhury, S. 1991, MNRAS, 252, 394
dell'Antonio, I. P., Geller, M. J. & Fabricant, D. G. 1995, AJ, 110, 502
Dressler, A. & Shectman, S. A. 1988, AJ, 95, 985
Edge, A. C., Stewart, G. C., Fabian, A. C., & Arnaud, K. A. 1990, MNRAS, 245, 559
Edge, A. C., Stewart, G. C., & Fabian, A. C. 1992, MNRAS, 258, 177
Evrard, A. E. 1988, MNRAS, 235, 911
Evrard, A. E. 1990, ApJ, 363, 349
Evrard, A. E. 1997, MNRAS, in press (astro-ph/9701148)
Evrard, A. E., Metzler, C. A. & Navarro, J. F. 1996, ApJ, 469, 494
Fabian, A. C. 1994, ARA&A, 32, 277
Fabian, A. C., Crawford, C. S., Edge, A. C., & Mushotzky, R. F. 1994, MNRAS, 267, 779
Fabricant, D. G. Beers, T. C., Geller, M. J., Gorenstein, P., Huchra, J. P. & Kurtz, M. J. 1986, ApJ, 308, 530
Fabricant, D. G., Kent, S. & Kurtz, M. J. 1989, ApJ, 336, 77
Geller, M. J. & Beers, T. C. 1982, PASP, 92, 421
Henriksen, M. J. & Markevitch, M. L. 1996, ApJ, 466, L79
Henry, J. P. & Briel, U. G. 1995, ApJ, 443, L9
Hughes, J. P., Butcher, J. A., Stewart, G. C. & Tanaka, Y. 1993, ApJ, 404, 611
Johnstone, R. M., Fabian, A. C., Edge, A. C. & Thomas, P. A. 1992, MNRAS, 255, 431
Jones, C. & Forman, W. 1984, ApJ, 276, 38
Jones, C. & Forman, W. 1992, in *Clusters and Superclusters of Galaxies*, NATO ASI, VOl 366, ed. A. C. Fabian (London: Kluwer), 49
Jørgensen, I. Franx, M. & Kjærgaard, P. 1996, MNRAS, 280, 167
Markevitch, M. 1996, ApJ, 465, L1
Markevitch, M. & Vikhlinin, A. 1997, ApJ, 474, 84
Matsuzawa, H., Matsuoka, M., Ikebe, Y., Mihara, T. & Yamashita, K. 1996, PASJ, 48, 565
Metzler, C. A. & Evrard, A. E. 1994, ApJ, 437, 564
Metzler, C. A. & Evrard, A. E. 1997, in preparation
Mitchell, R. J., Dickens, R. J., Bell Burnell, S. J., & Culhane, J. L. 1979, MNRAS, 189, 329
Mohr, J. J., Evrard, A. E., Fabricant, D. G. & Geller, M. J. 1995, ApJ, 447, 8
Mohr, J. J., Geller, M. J. & Wegner, G. 1996, AJ, 112, 1816
Mohr, J. J. & Wegner, G. 1997, AJ, in press (astro-ph/9704202)
Mohr, J. J. & Evrard, A. E. 1997, in preparation
Mushotzky, R. F. & Scharf, C. A. 1997, ApJ, 482, L13
Navarro, J. F., Frenk, C. S. & White, S. D. M. ApJ, 462, 563
Pildis, R. A., Bregman, J. N. & Evrard, A. E. 1995, ApJ, 443, 514

Press, W. H., Teukolsky, S. A., Vetterling, W. T. & Flannery, B. P. 1992, Numerical Recipes in C, 2nd Edition, (Cambridge University Press, Cambridge)
Roettiger, K., Burns, J. O. & Loken, C. 1996 ApJ, 473, 651
Schindler, S. 1996, A&A, 305, 756
Smith, B. W., Mushotzky, R. F., & Serlemitsos, P. 1979, ApJ, 227, 37
Snowden, S. L., McCammon, D., Burrows, D. N. & Mendenhall, J. A. 1994, ApJ, 424, 714
Tamura et al. 1996, PASJ, 48, 671
White, S. D. M., Navarro, J. F., Evrard, A. E. & Frenk, C. S. 1993, Nature, 366,429
Zabludoff, A. I. & Zaritsky, D. 1995, ApJ, 447, L21

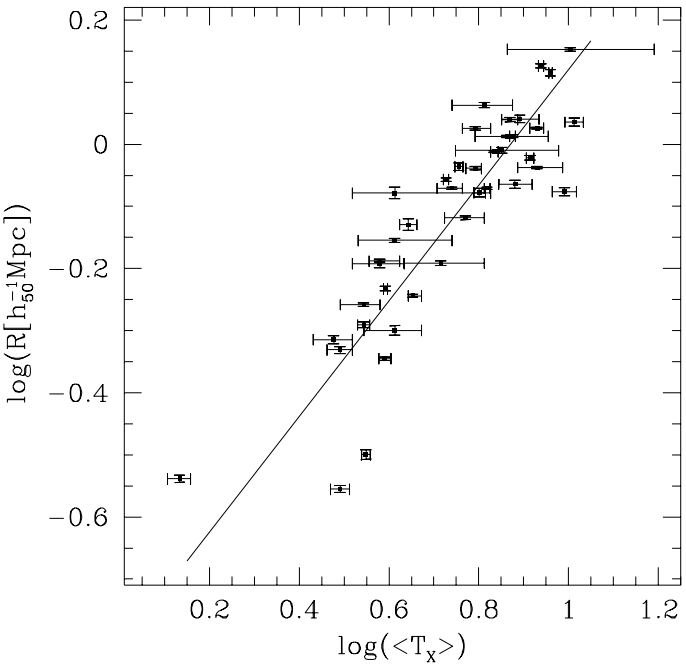

FIG. 1.— The X–ray ST relation for 41 clusters. The cluster redshift is used to calculate R_I , and $I = 1.93 \times 10^{-3}$ cts/s/arcmin^2; error bars are 1σ. The best fit ST relation (see Eqn 2-2) is plotted, and the *rms* scatter around this relation is $\delta \log R_I = 0.084$. The intrinsic scatter about the relation (removing contribution from $\langle T_X \rangle$ uncertainties) is $\delta \log R_I = 0.064$ (15%); for 30 clusters with $\langle T_X \rangle > 4$ keV, the scatter is $\delta \log R_I = 0.041$ (10%).

TABLE 1
GALAXY CLUSTER DATA

Cluster	t_{exp}[a]	I_B[b]	R_I[c]	$\langle T_X \rangle$[d]	Flow
A262	8.1	3.31	0.289	1.36	X
MKW3s	9.2	5.80	0.485	3.00	X
A1060	14.6	5.34	0.279	3.10	
A2052	5.9	6.06	0.467	3.10	X
A1367	17.7	3.07	0.512	3.50	
A4059	5.2	2.90	0.552	3.50	
A3526	3.0	7.09	0.317	3.54	X
A3562	18.5	4.19	0.643	3.80	
A780	17.3	2.34	0.649	3.80	X
AWM7	12.6	3.34	0.452	3.90	X
A496	8.1	3.82	0.586	3.91	X
A2063	9.6	6.90	0.502	4.10	X
A3112	7.2	2.64	0.700	4.10	X
CygA	8.7	7.07	0.835	4.10	X
A2147	0.9	6.40	0.743	4.40	
A2199	9.7	2.79	0.570	4.50	X
A3391	5.5	3.24	0.644	5.20	
A1795	24.8	3.09	0.878	5.34	X
A3158	2.9	2.60	0.850	5.50	
A3558	27.8	4.75	0.920	5.70	
A119	14.3	2.82	0.761	5.90	
A3266	7.0	3.35	1.061	6.20	
A85	5.3	3.18	0.915	6.20	X
A426	4.4	7.40	0.836	6.33	X
A3667	11.3	4.39	1.156	6.50	
A644	9.5	2.18	0.849	6.59	
A478	21.4	1.48	0.973	6.84	X
A2244	2.9	2.31	0.978	7.10	
A2255	12.5	2.11	1.030	7.30	
A399	6.4	2.29	1.096	7.40	
A2256	17.1	2.61	1.030	7.51	
A3571	5.5	4.98	0.862	7.60	
A2029	11.9	5.94	1.098	7.80	X
A1656	19.4	5.21	0.951	8.21	
0745-19	9.1	1.97	0.917	8.50	X
A754	6.1	2.41	1.062	8.50	
A2142	4.8	2.65	1.337	8.68	X
A2319	2.9	4.92	1.303	9.12	
Ophi	3.7	6.38	0.839	9.80	
A1689	13.3	2.53	1.422	10.10	
Tria	6.6	4.20	1.086	10.30	

[a]Exposure [ks]

[b]Background [10^{-4} cts/s/arcmin^2]

[c][h_{50}^{-1} Mpc]

[d][keV]

TABLE 2
FIT RESULTS FOR SIZE–TEMPERATURE RELATION

Source	I^{a}	m	b	$\delta \log R^{b}$
PSPC	9.65	0.886 (0.124)	-0.030 (0.013)	0.074
PSPC	19.3	0.934 (0.109)	-0.080 (0.013)	0.064
PSPC	38.6	1.047 (0.130)	-0.204 (0.014)	0.069
PSPC	77.2	1.514 (0.382)	-0.356 (0.024)	0.151
SCDM	16.2	0.699 (0.035)	0.119 (0.013)	0.042
OCDM	66.4	0.612 (0.025)	0.111 (0.010)	0.054
LCDM	66.4	0.721 (0.024)	0.156 (0.007)	0.035
ZCDM	16.2	0.808 (0.067)	0.161 (0.022)	0.069

[a] $[10^{-4}$ cts/s/arcmin$^2]$

[b] Intrinsic scatter (corrected for errors in $\langle T_X \rangle$)

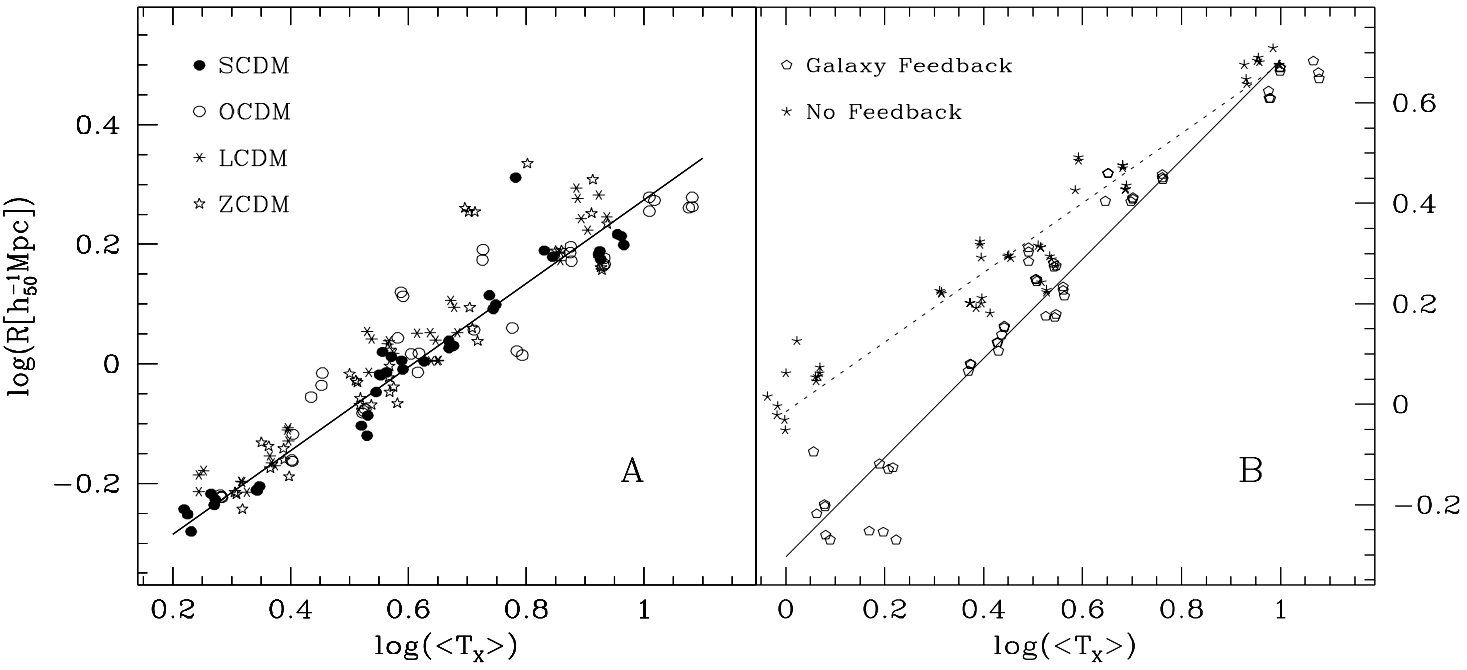

FIG. 2.— The ST relations for simulated galaxy clusters. Our 48 simulations appear on the left (A), with the points coded according to cosmological model. The best fit relation for the SCDM model is plotted (see Table 2), and the *rms* scatter around this relation is $\delta \log R = 0.042$. The scatter for these simulated clusters (which have formed recently) is similar to that for observed clusters, but the slope of the relation is shallower. On the right (B) we demonstrate the effects of galaxy feedback on the ST relation with simulations from Metzler & Evrard (1994, 1997). The best fit slope for the clusters simulated with feedback ($m = 0.99$) is much steeper than the slope of those simulated without feedback ($m = 0.69$).

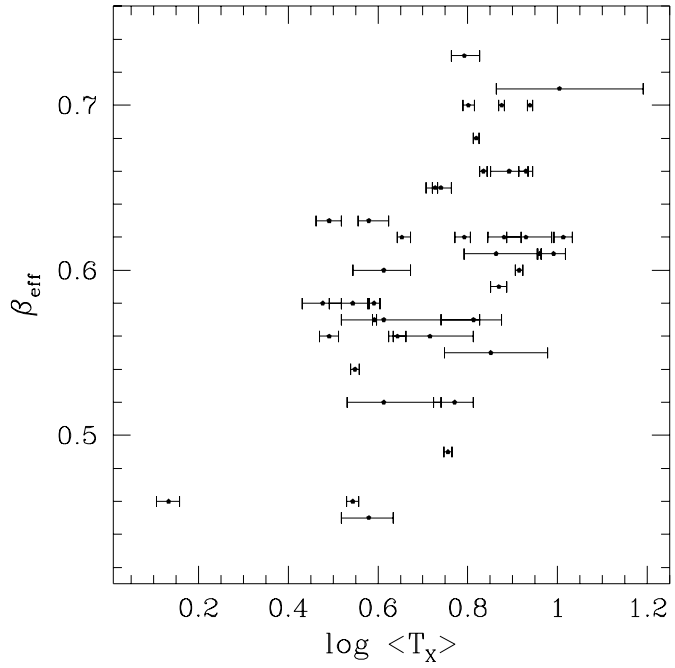

FIG. 3.— Slopes of the X–ray surface brightness profiles are plotted versus cluster temperature $\langle T_X \rangle$. The trend for cooler clusters to have shallower profiles is qualitatively consistent with the effects of galaxy feedback. β_{eff} is calculated independent of the cluster core radius and requires no azimuthal averaging (see §4.3 for details).